Micromagnetic Simulations with MuMax3

Nitin Jha

Ashoka University, Sonepat, Haryana

Abstract

MuMax is a GPU accelerated software which uses finite-difference method to solve various Micromagnetic systems by solving the *LLG* equation. This paper explores the theoretical information related to various energy terms for a micromagnetic systems, the working of MuMax, and analysing some system using it. This is achieved by obtaining the hysteresis loop for various systems.

1 Introduction

In spite of the early discovery of magnetic materials it took nearly three millenniums until a basic understanding of magnetism was possible. The history of magnetism has been treated by Mattis up to the quantum theory of the last century. Through various centuries various scientific theories developed our current understanding about magnetism. Maxwell developed the first formulation about the connection between electrical and magnetic phenomenon, static and dynamic, by the famous set of equations– Maxwell's equation. He introduced several types of magnetic fields by the equation,

$$B = \mu_0 H + J = \mu_0 (H + M) = \nabla \times A \qquad (1)$$

In the above equation, B : the magnetic flux density, H : magnetic field strength, M : the magnetization. In vacuum, $B = \mu_0 H$, where $\mu_0 = 4\pi \cdot 10^{-7}\ Vs/Am$. The solutions of Maxwell's equations, requires the knowledge material law, i.e.,

$$J = (\mu - I)\mu_0 H \implies \mathbf{M} = \chi \cdot \mathbf{H} \qquad (2)$$

In the above equation, χ is the magnetic susceptibility and is given as, $\chi = d\mathbf{M}/d\mathbf{H}$. Many efforts are being made each day towards understanding various properties associated with magnetic materials. The ever growing interest in magnetic materials, and their application has led to significant development of both the experimental, and the computational methods to understand these systems with a greater clarity.

The previously known theory about micromagnetism were applicable to the crystalline materials based on transition metals and garnets. However, the development of various new ferromagnetic materials such as *nano-crystalline* and amorphous alloys as well as *inter-metallic compounds* have opened the horizons for understanding the properties such as *Curie temperature*, critical exponents, and various other properties because of the static fluctuations of intrinsic microscopic magnetic properties.

1.1 The Micromagnetic Approach

The micromagnetic theory is an approach to describe magnetization reversal, i.e. the magnetization state evolution due to sweeping the magnitude of the applied field from one extremum to its

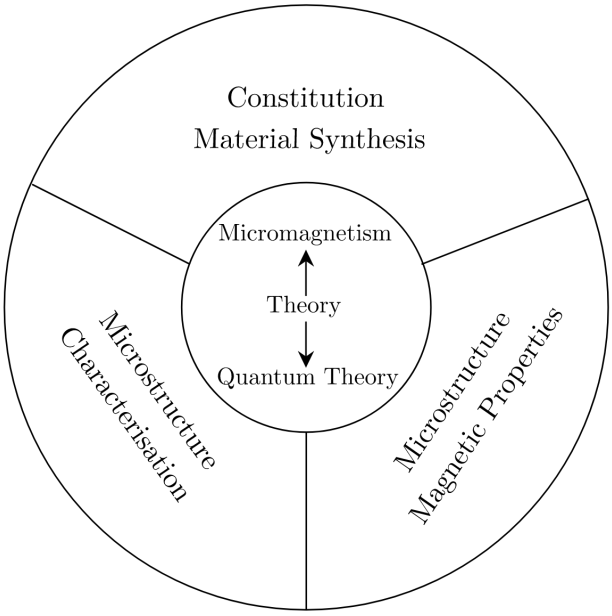

Figure 1: *A schematic representation of interdisciplinary cooperation for developing and analysing various magnetic materials.[1]*

opposite value, and thus hysteresis of a magnet at length scales between magnetic domains and crystal unit cells. [2]
Due to the large number of cells that require solving the magnetization dynamics, the micromagnetic description of a system is generally employed in numerical methods that describe the time-evolution of the system in terms easily "understood" by a computer. Solving these equations have been well researched, and

2 Background Theory

In this section, we shall discuss some important theoretical understanding co-related to the work presented in this paper.

2.1 The Origin of Magnetization

The concept and description of magnetic materials dates back to 6^{th} century as naturally occurring magnetic materials such as Lodestone. [3] Throughout centuries this phenomenon was studied extensively, however the greatest advancement in magnetism were made as a result of the development of our understanding about the wave particle duality, and the significant advancement in the field of quantum mechanics.

2.1.1 The Magnetic Dipole Moment

From a classical perspective, the motion of the electron (charge) in the vicinity of the nucleus can be considered an Ampérian loop that gives rise to a magnetic dipole moment. A schematic representation of a magnetic dipole is given below, Mathematically, magnetic dipole can be written

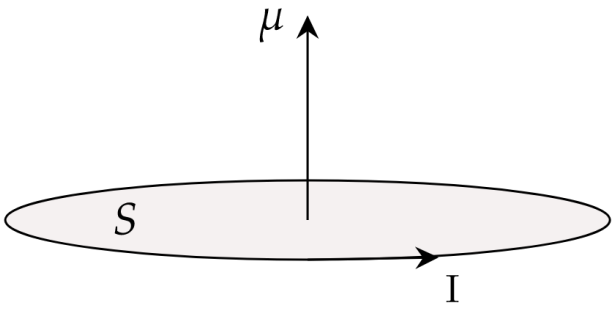

Figure 2: *Schematic representation of atomic magnetic dipole.*

as,

$$\mu = \int I \cdot d\mathbf{S} \tag{3}$$

In the above equation, μ is the magnetic dipole moment, I is the current flowing through the loop of area $\mathbf{dS}$. Considering the angular momentum of electron, we can write the magnetic dipole moment as,

$$\mu = \alpha \mathbf{L} \tag{4}$$

A schematic diagram of atomic orbital for single electron is displayed below,

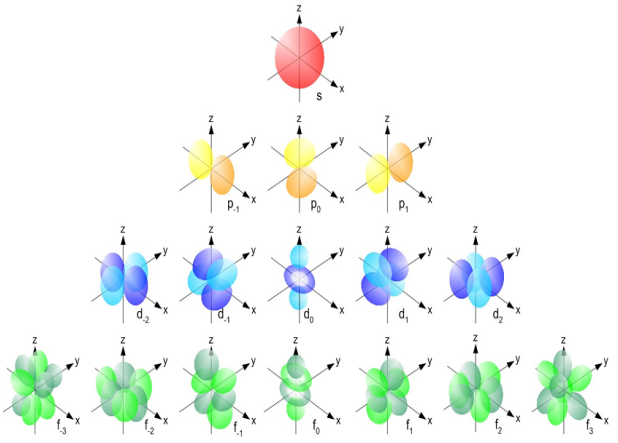

Figure 3: *Atomic orbital for a single electron. [4]*

2.1.2 Quantum Approach to Magnetism

The theoretical framework considers electron as a probability distribution over the available space,

rather than being at a fixed position. This probability function is given by l (azimuthal quantum number), and m_l (magnetic quantum number). This probability distribution of electron in an atom are known as orbitals. Considering an electron in an orbit, the magnitude of μ can be found as,

$$|\mu| = -\frac{e}{2m_e} vRm_e \tag{5}$$

The term vRm_e is the orbital angular momentum of the electron. The magnetic quantum number can take all the integer values between $-l$ and , $+l$ giving $(2l+1)$ different available orbitals. The magnitude of magnetic moment of the electron that has an orbital angular momentum of exactly $\hbar$ is defined as the Bohr magneton,

$$\mu_B = \frac{e\hbar}{2m_e} \tag{6}$$

The Bohr Magneton is used as a unit to describe magnetic moments. The value of Bohr Magneton is, $\mu_B = 9.274 \times 10^{-24}\ Am^2$. The magnitude of the magnetic dipole moment of an electron in an atomic sub-shell characterized by the quantum numbers (l,m_l) is $\sqrt{l(l+1)}$ its projection along a given axis is given by $m_l \mu_B$.

2.1.3 Magnetic Solids

We can define a new quantity, the magnetization M, which in the continuum approximation, is a smooth vector field representing the spatial density of the magnetic dipole moment. In vacuum, for an applied magnetic field H, the measured magnetic field B is simply the product of the former with a the magnetic permeability of free space μ_0,

$$\mathbf{B} = \mu_0 \mathbf{H} \tag{7}$$

Now, we can write M in terms of H using magnetic susceptibility as,

$$\mathbf{M} = \chi \mathbf{H} \tag{8}$$

The value of χ can be used to define different classes of materials. For diamagnetic materials: $(\chi < 0)$, paramagnetic materials: $(0 < \chi << 1)$, ferromagnetic materials: $(\chi >> 1)$. One apparent consequence of the proportionality between M and H is that the magnetization can grow indefinitely with increasing applied magnetic field. By the definition of the magnetization, there must be a value for which all magnetic moments in the considered volume are aligned, thus providing an upper bound for M, known as *saturation magnetization*.

2.1.4 Ferromagnets

In ferromagnetic materials, the observed dependence of the magnetization on the magnetic field strength is non-linear and dependent on the sign of the change in H. Thus, the nature of the curve obtained for positive and negative values of H will be different. A useful way to study this is by studying the closed nature graph obtained by sweeping H from negative to positive values. This closed loop graph is known as hysteresis loop. We can notice the important properties of magnetic materials by observing it's hysteresis loop, For this

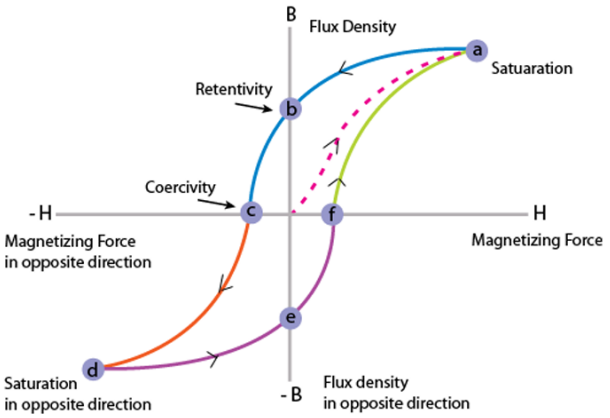

Figure 4: *Hysteresis loop for a ferromagnetic showcasing all the points of interest.*

paper, hysteresis loop serves as the major source of information. These curves will help us understand the behavior of various systems studied for this particular project.

In a ferromagnet, the various spin interactions introduce energy costs of different magnitudes that compete to give the ground state of the magnetic system In ferromagnets, a "puzzle"-like structure of regions in which the magnetization is co-linear and locally reaches saturation, yet its orientation is different in each respective region. These regions are known as domains, and these are the main reasons we see the hysteresis curves that we discussed earlier. A schematic of these intrinsic domains is displayed below,

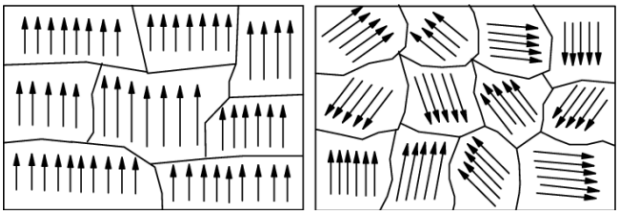

Figure 5: *Two magnetic configurations are shown above. On left, we can see that the domains are aligned in one direction, indicating a presence of non-zero magnetization. On right, we see that the domains are not aligned in particular direction, hence no overall magnetization.[5]*

2.2 Energy Terms of Magnetic Interactions

There are various energy terms associated with the spin interactions of the electrons in the magnetic domain.

2.2.1 Heisenberg Exchange Energy

The exchange interaction is the phenomenon that favours parallel alignment of neighbouring spins and is the deciding factor in ferromagnetic ordering. In a magnetic solid, the exchange interaction acts between all pairs of neighbouring atoms, promoting the so called Heisenberg model. The Hamiltonian in this case is expanded to,

$$\mathscr{H} = -2 \cdot \sum_{i>j} \mathbf{S_1} \cdot \mathbf{S_2} \tag{9}$$

In eq(9) $i > j$ takes care for the over-counting of the spin pairs. The calculation of the exchange integral depends on the choice of electrons to be considered as well as the crystal environment such that a number of well studied exchange interactions can be defined

2.2.2 Magnetocrystalline Anisotropy Energy

The expression of the Heisenberg Hamiltonian is isotropic with respect to the crystal axis, as the the spin quantization axis does not have any spatial restrictions. This assumption does not suffer from loss of generality, but empirical evidence suggests that the magnetization does have a preferred direction of alignment, rather should depend on the crystalline environment. This is known as magneto-crystalline anisotropy. This mainly arises due to the correction to our previous Hamiltonian by including the effect such as spin-orbit coupling, dipole-dipole interaction as this breaks the rotational symmetry of the spin quantization axis. [6] The crystal anisotropy energy term must be a spatial function with the magnetization as an argument and as coefficients, some angular relation between the magnetization and the crystallographic axes. Thus we can write a power series in terms of the direction cosines, α_1, α_2, α_3 as,

$$E_{anis} = b_0 + \sum_{i=1,2,3} b_i \alpha_i + \sum_{i,j=1,2,3} b_i \alpha_i \alpha_j + \dots \tag{10}$$

where $(\alpha_1, \alpha_2, \alpha_3) = (\sin\theta\cos\phi, \sin\theta\sin\phi, \cos\theta)$ with θ, ϕ the polar and azimuthal angles respectively. Moreover, experimental investigations show that the energy contribution of higher order terms in the expansion are compensated with thermal noise, such that mostly the first six order terms are included in the energy expression. As the energy cost associated with magneto-crystalline anisotropy is dependent on the crystal environment, it is expected that the formula takes a different expression for each crystal lattice. More accurately, it is the symmetry of the crystal environment that dictates the final form of the energy expression.

2.2.3 External Field Energy (Zeeman)

This term represents the energy cost of misalignment between an applied magnetic field and the magnetic moment of the sample. Consider a single spin with magnetic moment μ in a field H. The Hamiltonian in this case can be written as,

$$\mathscr{H} = \mu_0 \mu \cdot \mathbf{H} \tag{11}$$

In the continuum approximation, total *Zeeman Energy* for a system can be written as,

$$E_{Zeeman} = -\mu_0 M_s \int \mathbf{H} \cdot \mathbf{m} dV \tag{12}$$

2.2.4 Stray Field Energy (Demagnetization/Magnetostatic)

In addition to the external applied field, the magnetization of the sample also creates a magnetic field inside the bulk, that opposes the field that created the magnetization in the first place. This secondary field also introduces an energy term. The demagnetizing (demag for short) field Hd can be thought to originate from the magnetic

"*monopoles*"accumulating in the volume and on the surface of the sample.[7] Thus the following set of equations should make sense,

$$\nabla \cdot \mathbf{H}_d = \nabla \cdot \mathbf{M} \tag{13}$$

$$\nabla \times \mathbf{H}_d = 0 \tag{14}$$

From eq(13), and eq(14) we can conclude the following,

$$\mathbf{H}_d = -\nabla \phi \tag{15}$$

Where ϕ is some magnetic scalar potential. The calculation of the demagnetizing field and the respective energy is complex and generally calls for numerical evaluation, except in the most simple cases, such as an infinitely extended plate or an uniformly magnetized ellipsoid.
The stray field is mainly responsible for the formation of domains and domain walls inside a magnetic sample, with exceptions arising in special cases of shape, size and anisotropy. The same complexity argument that arises in the calculation of the demag-field is taken over to the calculation of domains and other magnetic textures. Numerical methods adapted for simulating magnetization dynamics consequently become an indispensable tool in the exploration of magnetic domains

3 Magnetic Skyrmions

3.1 Basic Definition

Magnetic Skyrmions are curling regions of topological defects in magnetic systems. The spins inside a skyrmion rotate progressively with a fixed chirality from the up direction at one edge to the down direction at the centre, and then to the up direction again at the other edge. There are two possible types of skyrmions, *Neel Skyrmion* and *Bloch Skyrmion* as shown in fig(6) and fig(7).

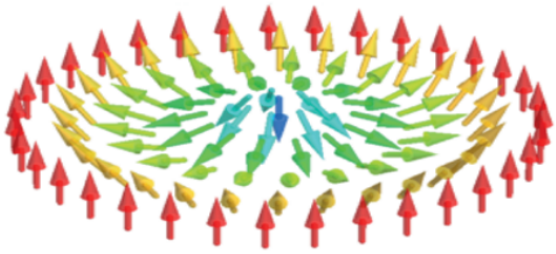

Figure 6: *A Neel type skyrmion.[7]*

In most systems, the spin configuration of skyrmions is determined by chiral interactions of

Figure 7: *A Bloch type skyrmion. [7]*

the Dzyaloshinskii–Moriya. Even though other types of localized whirling magnetic textures, such as magnetic bubbles, can be stabilized without Dzyaloshinskii– Moriya interactions (DMIs). Skyrmions can, indeed, be defined by the topological number S (or skyrmion number), which is a measure of the winding of the normalized local magnetization, m. In the two-dimensional limit, the topological number is,

$$S = \frac{1}{4\pi} \int \mathbf{m} \cdot (\partial_x m \times \partial_y m) \underset{\cdot}{\mathrm{xy}} = \pm 1 \tag{16}$$

Magnetic skyrmions were initially identified in single crystals of magnetic compounds with a non-centrosymmetric lattice, and explained by the existence of DMIs induced by spin–orbit coupling in the absence of inversion symmetry in the crystal lattice. But without the presence of symmetry in the system, the presence of Interfacial Dztaloshinskii-Moriya Interaction can also result in a stable skyrmion.

3.2 Interfacial Dzyaloshinskii–Moriya interaction

The presence of spin–orbit coupling can induce an asymmetric exchange interaction, the DMI, which takes the following form,

$$H_{DMI} = (\mathbf{S}_1 \times \mathbf{S}_2) \cdot \mathbf{d}_{12} \tag{17}$$

where S_1 and S_2 are neighbouring spins and d_{12} is the corresponding Dzyaloshinskii–Moriya vector. For $d_{12} > 0$ the DMI favours anticlockwise rotations from S_1 to S_2, and $d_{12} < 0$ the DMI favours clockwise rotations from S_1 to S_2.

4 Micromagnetic Simulations

4.1 Micromagnetic Equations

There exists an equation that dictates the dynamics of the magnetic moments in a solid. The formulation is credited to *Lev Landau* and *Evgeny Lifshitz*, which is why the equation is also referred to as the *Landau-Lifshitz equation*. It originates from the same variational principle already described in earlier sections.
The effective field contains all the various magnetic considerations of interest to the goal of this paper. In static equilibrium, $M \times H_{eff} = 0$, i.e. the torque on the magnetization must vanish at all points and consequently, the magnetization must be directed along the effective field vector. If the torque does not vanish, it will dictate the time evolution of the magnetization field, modulated by the gyromagnetic ratio, γ of the electron. This can be represented mathematically as,

$$\frac{d\mathbf{m}}{dt} = -\gamma(\mathbf{m} \times \mathbf{H_{eff}}) \tag{18}$$

One may recognize this expression as describing precession of the magnetization vector about the effective field. In this form, the angle between the two remains constant and the precessional motion continues indefinitely. This feature arises from the fact that no energy losses have been taken into account. By including an additional term in eq(18) that describes local dissipative phenomena, one arrives to the Landau-Lifshitz-Gilbert (LLG) equation,

$$\frac{d\mathbf{m}}{dt} = -\gamma_{LL}(\mathbf{m} \times \mathbf{H_{eff}}) + \alpha_{LL}\mathbf{m} \times (\mathbf{m} \times \mathbf{H_{eff}}) \tag{19}$$

Where, $\gamma_{LL} = \gamma/(1+\alpha_G^2)$, and $\alpha_{LL} = \alpha_G\gamma/(1+\alpha_G^2)$, and where α_G is the *Gilbert damping coefficient*. Using this expression, it is possible to obtain the state of equilibrium of the magnetic system and implicitly the evolution of the magnetic texture under various time-dependent perturbations.

4.2 MuMax^3: Numerical Method, Features, and Capabilities

The micromagnetic simulation program MuMax3 allows for the computation of magnetization dynamics as well as the magnetization response to an applied magnetic field and various other excitations. In order to do that, the software makes use of the graphics-processsing-unit (GPU), due to its excellent capability for parallelization, a quality which is required for optimally resolving 2-dimensional magnetic textures. The software

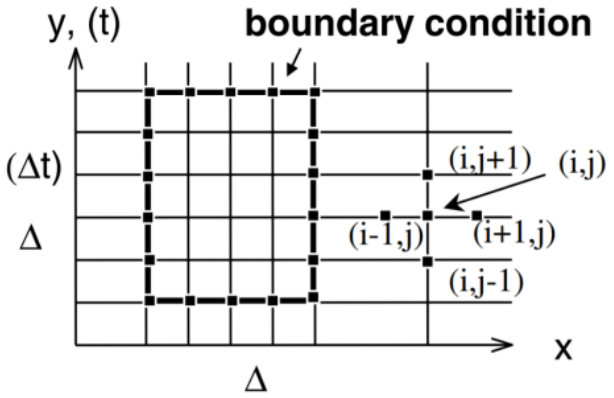

Figure 8: *Schematic diagram for the finite difference method using a mesh grid.*

employs a finite-difference spatial discretization, thus dividing the simulation space into equal sized cells. Due to the many interactions present when solving the micromagnetic equation, the quantities of interest can be divided into two categories, base on the relation that they modulate. Volumetric quantities, such as the magnetization and the effective field are treated at the center of each cell, while coupling quantities which represent relative interactions are considered at the faces of each cell. Due to memory saving considerations, these former quantities are not saved for each cell, rather material regions are defined which encompass more than one cell, and the specific material parameters are saved per each region instead. Due to the same reason, coupling quantities are saved in a triangular matrix.

4.3 Numerical Approach

As mentioned in earlier sections, MuMax3 employs a finite difference method. The premise of this method is that a differential equation of the form can locally be approximated as a sum of finite difference quotients.

5 Results

In this section, I'll present some of the *hysteresis loops* for a variety of systems, velocity profile for the *U-branch* racetrack, and brief discussion of the

problems associated with a horizontal racetrack with multiple skyrmions in it.

5.0.1 Material Parameters

- $M_{sat} = 580 \cdot 10^3 B$
- $A_{ex} = 15 \cdot 10^{-12}$
- $DMI = 3.2 \cdot 10^{-3}$
- $KU_1 = 0.9 \cdot 10^6$

The value of α and β, i.e., coefficient of adiabaticity are adjusted to control the motion of the skyrmion.

5.1 Part I: Hysteresis Loops

For magnetic systems, the hysteresis loop is an important way to study the nature of these systems. When we apply external magnetic field, the flux density (B) increases from one point and saturates at a particular value (1), and then as we decrease the external magnetic field, we often find the direction of the flux density (B) getting reversed and saturate in the oposite direction (i.e., -1). We plotted hysteresis curve for a simple system at two different temperatures, and then two systems containing skyrmions.

5.1.1 Two cubes joined to each other

We take two cubical regions of dimensions $1000 \times 1000 \times 3\ nm^3$, and then we add both of the regions together using the function *c1.add(c2)*. Then we vary the external magnetic field from $-1\ T$ to $1\ T$ along the y-direction, and record the change in magnetisation value along the same direction. The following are the hysteresis curves obtained for this particular system, i.e., fig(10) and fig(9)

Here, we see a perfect hysteresis loop at $0K$, but we seem to be missing one part of the curve at $100K$. One may ask, why that's the case? The answer is rather simple– it's nothing to do with the system but rather with the computational power of the system used. The current hysteresis curve took about 12 *hrs* each! So, if we can run the system for longer time or on a computationally powerful device, we'll in-fact see the final complete loop as we see for $T = 0K$ case.

5.1.2 Simple System with Skyrmions

We take a simple magnetic domain and insert a domain at the centre of the magnetic region. Then

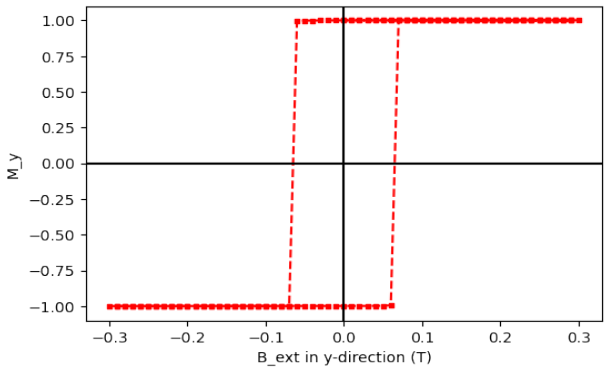

Figure 9: *Hysteresis curve of bi-cuboidal system described above at $T = 0K$*

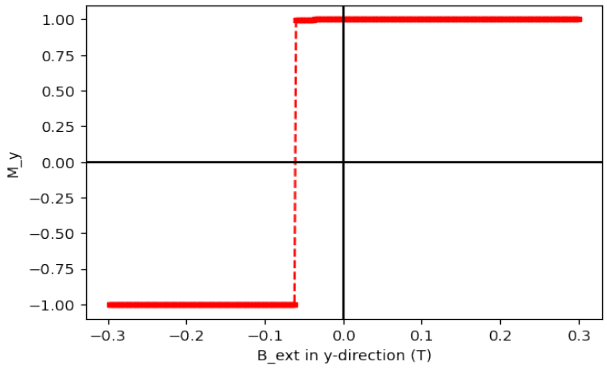

Figure 10: *Hysteresis curve of bi-cuboidal system described above at $T = 100K$*

we vary the external magnetic field from $-0.1\ T$ to $0.1\ T$ along the y-direction, and record the change in magnetisation value along the same direction. The following are the hysteresis curves obtained for this particular system,

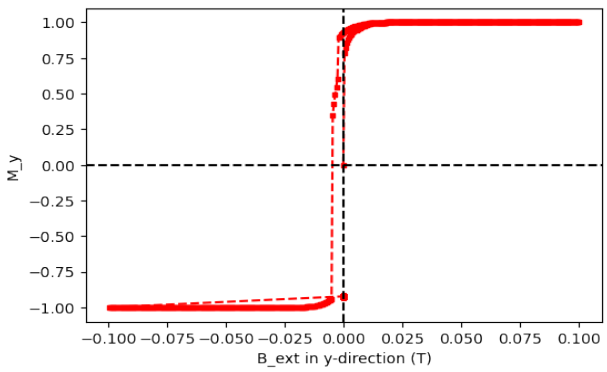

Figure 11: *Hysteresis curve for a system with a skyrmion at $T = 100K$*

Here we notice that the width of the hysteresis loop is lesser than that of the system without a skyrmion. Now, we also notice that the width of the hysteresis curve decreases even further as

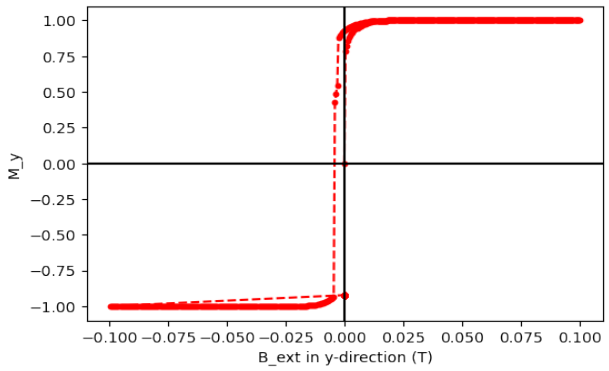

Figure 12: *Hysteresis curve for a system with a skyrmion at $T = 100K$*

we change the temperature from $T = 0K$ to $T = 100K$. This is in accordance with the earlier tested theories mentioned in various articles.

5.1.3 U-shape Racetrack

Moving forward we started to work on Racetrack systems. We begun by analysing L-shaped racetrack, the size of the simulated system is $256 \times 256 \times 1\ ns^3$. Analysis of the system didn't yield good enough result to be published here, but it gave us the idea about working with systems with skyrmion and how to move the skyrmion with an external current. First of all, we start by plotting the hysteresis curve for U-shaped system. The following is the U-shape branch used for this simulation,

Figure 13: *U-shape system used for simulation for this section*

Now, in the above system we installed a skyrmion in the left hand of the U-shaped race track. The system looks like the following,
Then we vary the external magnetic field from $-0.1\ T$ to $0.1\ T$ along the z-direction, and record the change in magnetisation value along the same direction. The following are the hysteresis curves obtained for this particular system,

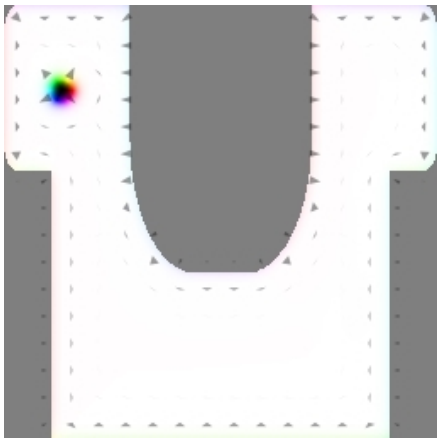

Figure 14: *U-shape system with a skyrmion in the left arm.*

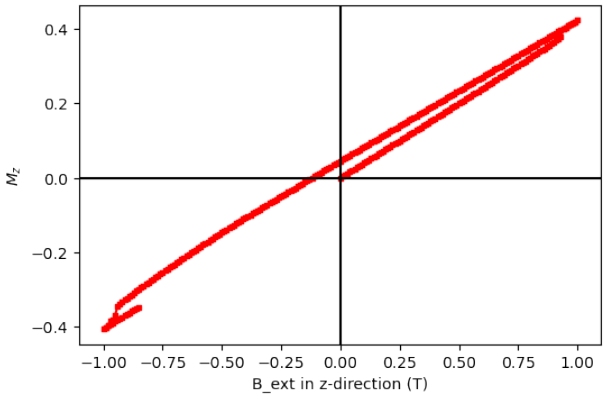

Figure 15: *Hysteresis loop for U-shape system with a skyrmion in the left arm of the magnetic region.*

Now, from the above graph we can notice a prominent thing from the graph. We notice that even after putting an external field as high as $B = 1T$ the magnetic flux density is not saturating at ± 1. This is mainly as the skyrmion is topologically protected, and one needs to apply certain amount of energy to overcome this barrier. This can be one of the reasons for the hysteresis curve not being a $S-$shaped curve.

5.2 More about the Racetracks

Now, we still work with the racetrack described above, but to gain an idea about how skyrmion moves in the system for a given current, we look at an L-shaped racetrack first. The following is a representation of the L-shape system used in the simulation in fig(16).
Now, we put a skyrmion in the L-shape system and put a current in the x-direction and it's magnitude

Figure 16: *L-shaped system used for the initial simulations.*

is of order $10^1 1$ A and the velocity profile is shown in fig(17). Then we placed two skyrmion in the system, and the velocity profile of the skyrmion is plotted in fig(18)

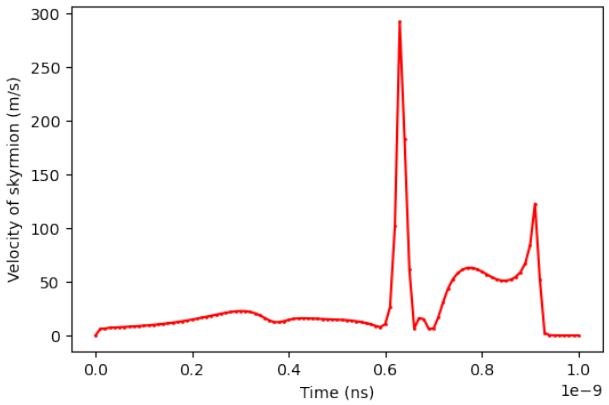

Figure 17: *Velocity profile for a single skyrmion in L-shaped system.*

From the figures we can notice one thing, the peak of the velocity curves decreased for a system containing two skyrmions.This can be associated with the skyrmion-skyrmion force. Now, we move on to work with U-shape racetrack again. For the hysteresis observing external magnetic field, we find the data for total energy of the system, and the Zeeman energy. Here, we plot the two energy term mentioned along with the velocity profile for the U-shaped race track in fig(19).
Fig(20) and fig(21) represent the graphs for the energy terms for the U-shaped systems. Zeeman energy, or the external field energy, is the potential energy of a magnetised body in an external magnetic field. It is named after the Dutch physicist

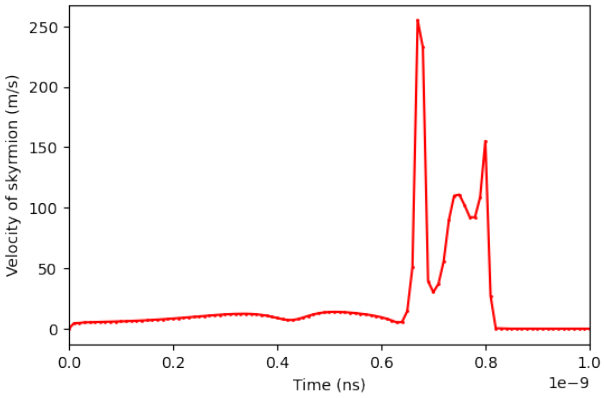

Figure 18: *Velocity profile for two skyrmion in L-shaped system.*

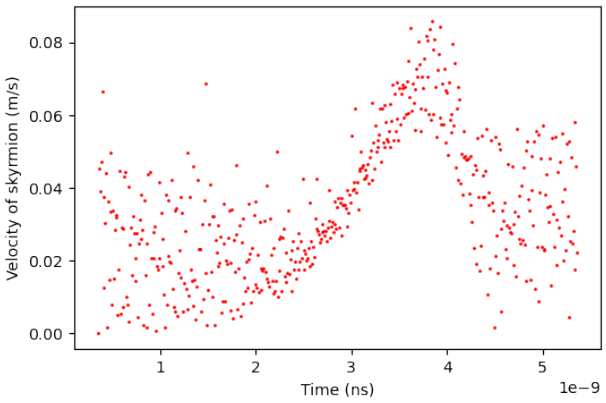

Figure 19: *Velocity profile for a single skyrmion in U-shaped system.*

Pieter Zeeman, primarily known for the Zeeman effect. Whereas, total energy of the system is just summation of all of the energy associated with the system in use.

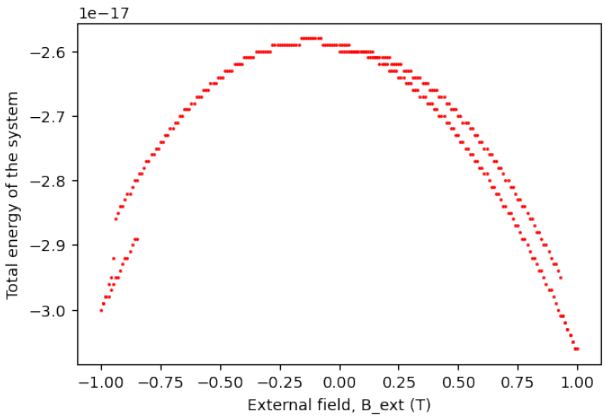

Figure 20: *Total energy of the system with a single skyrmion in U-shaped system.*

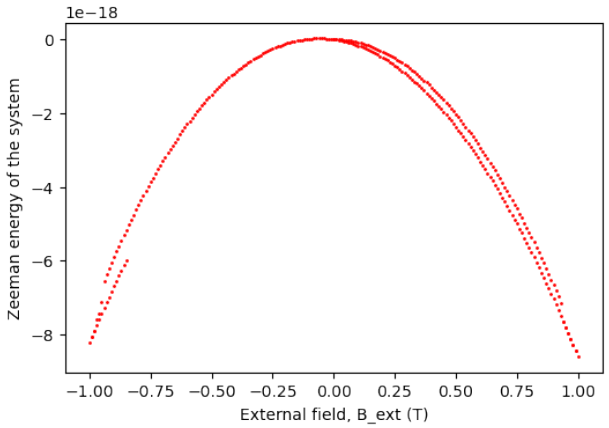

Figure 21: *Zeeman energy of the system with a single skyrmion in U-shaped system.*

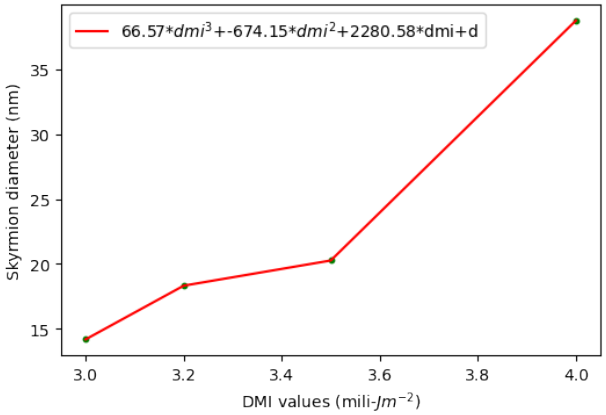

Figure 22: *Changing DMI values and observing the change in diameter of the skrymion in the U-shape system*

One of the important things to note in fig(19) is that even for currents of the order 10^{11}, the magnitude of the velocity of the skyrmion in the system is of the order 0.01 m/s. This is one of the major problems in constructing a U-shaped race track. Even after tuning the various materials parameters, we never notice that the velocity of the skyrmion reach of the order of 100 m/s or so which is physically required to make this effective. Furthermore the spread of the velocity profile can be assocaited with the noise in the system due to high values of current being passed. As such high values of current are passed, it heats up the system and hence altering some of the intrinsic property of the material being simulated.

5.2.1 Skyrmion's diameter and DMI values

Now, we see the change in the value of the diameter of the skyrmion in a relaxed state in a U-shape system. The system was simulated using MuMax and relaxed to find the size of skyrmion using ImageJ. Fig(22) represents the change in size of the skyrmion with respect to change in DMI values,
Now using the modelled equation found from the previous data, the change in skyrmion's diameter with respect to DMI values is modelled in fig(24). For our system (i.e., $256 \times 256 \times 1$ ns^3), we notice from the graph that the suitable values of DMI is between $2e-3$ and $4e-3$ units.

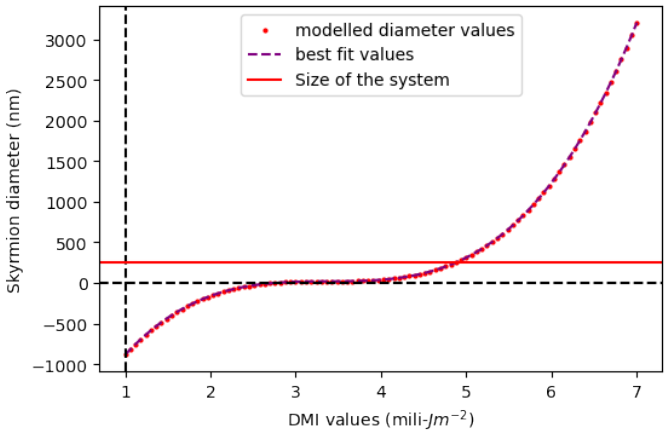

Figure 23: *Modelled change in skyrmion's diameter with changing DMI values in the U-shape system*

5.3 Horizontal Racetrack with three Skyrmions

In this section, we'll see how the size of skyrmion changes in a horizontal race-track where there's skyrmion-skyrmion interaction in the system. Fig(**??**) shows the two state of horizontal race track with 3 skyrmions in it.

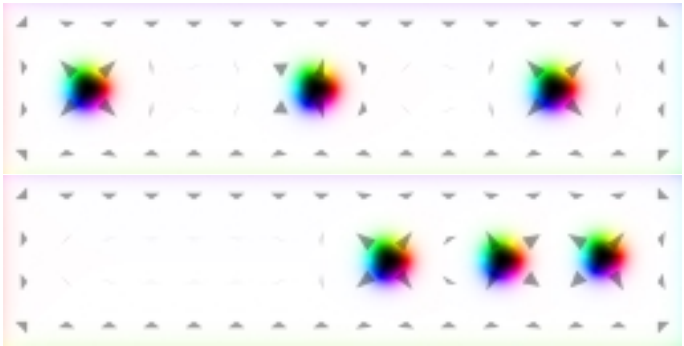

Figure 24: *Multiple skyrmion in horizontal racetrack.*

From the observation above, we can see that by the end of the simulation time the distance between each skyrmion decreased from 80nm to 5 nm and

8 *nm*. We also notice that the size of the skyrmion reduced from 16 *nm* to 12 *nm* towards the end of the track. This can be avoided by installing notches at the end of the end of the tracks. [8]

6 Concluding Remarks

In this study, we learned the basics of MuMax simulations. The initial simulations were to understand the basic structure of the coding files, and learning the basics of algorithms used in MuMax. Then we moved on to simulations basic systems, skyrmionic-systems, domain wall systems, and various other on the way. Moving forward, we looked at L-shaped racetrack and studied the behavior of skyrmion installed in it. Then building up on the findings, we looked at the U-shaped race-track and studied the velocity profile for both of these systems. However, the major topic of study was Hysteresis curve of the various systems to see if there was magnetic reversal for the system. One important point from the hysteresis curve for the systems with skyrmion is that the system did not saturate to the maximum value, i.e., ± 1. We also noticed that the velocity of the skyrmion in the U-shape system is very low for larger value of current, i.e., current of the order $10^{11}\ A$. Larger values of current causes excessive heating to the system, and thus the practicality of the system is questionable.

7 Acknowledgement

I would like to acknowledge the constant support and guidance of Prof. Susmita Saha throughout this ISM. I would extend my gratitude to Riya Mehta, Vineet Tiwari and Satwik Wats for their help in various part of this project.

References

[1] Kronmüller Helmut, & Fähnle Manfred. (2009). Micromagnetism and the microstructure of ferromagnetic solids. Cambridge University Press.

[2] L. Si, Z. Zhong, J. M. Tomczak, and K. Held, "*Route to room-temperature ferromagnetic ultrathin srruo*$_3$3 *films*," Phys. Rev. B, vol. 92, p. 041108, Jul 2015.

[3] J. Keithley, The Story of Electrical and Magnetic Measurements: From 500 BC to the 1940s. Wiley, 1999.

[4] Libretexts, "Electronic orbitals," Jun 2019

[5] J. Souza and R. Jardim, "Electrical transport in disordered and ordered magnetic domains under pressures and magnetic fields," Journal of Physics D: Applied Physics, vol. 42, p. 032006, 01 2009.

[6] P. Bruno, Physical Origins and Theoretical Models of Magnetic Anisotropy. 01 1993.

[7] A. Hubert and R. Sch¨afer, Magnetic Domains: The Analysis of Magnetic Microstructures. Springer, 1998.

[8] Zhang, Xichao, G. P. Zhao, Hans Fangohr, J. Ping Liu, W. X. Xia, J. Xia, and F. J. Morvan. "Skyrmion-Skyrmion and Skyrmion-Edge Repulsions in Skyrmion-Based Racetrack Memory." Scientific Reports 5, no. 1 (January 6, 2015). https://doi.org/10.1038/srep07643.

[9] "The design and verification of mumax3", AIP Advances 4, 107133 (2014).